Journal of Solid State Chemistry **158,** 14–24 (2001)
doi:10.1006/jssc.2000.9048, available online at http://www.idealibrary.com on IDEAL®

On the Crystal Structure of $Ln_2O_2CO_3$ II (Ln = La and Nd)

Anja Olafsen,* Ann-Kristin Larsson,† Helmer Fjellvåg,*,[1] and Bjørn C. Hauback‡

*Department of Chemistry, University of Oslo, P.O. Box 1033 Blindern, N-0315 Oslo, Norway; †Inorganic Chemistry, Arrhenius Laboratories, University of Stockholm, S-106 91 Stockholm, Sweden; and ‡Institute for Energy Technology, N-2027 Kjeller, Norway

Received July 11, 2000; in revised form November 7, 2000; accepted December 8, 2000; published online March 8, 2001

The crystal structures of $La_2O_2CO_3$ II and $Nd_2O_2CO_3$ II have been shown by means of high-resolution powder neutron (PND) and synchrotron X-ray diffraction (SXRD) combined with selected area electron diffraction (SAED) studies to be far more complex than earlier anticipated, owing to ordering of carbonate groups between $(Ln_2O_2^{2+})_n$ layers. In contrast to earlier descriptions, the carbonate groups appear to be rather regular. Relative to an average model, the SAED patterns show additional scattering in the form of closely distributed, but essentially discrete, spots along $\langle\frac{1}{3}, \frac{1}{3}, l\rangle^*$. Most of the observed scattering, H, can be described as $\mathbf{H} = \mathbf{G} \pm m\mathbf{q}_1 + n\mathbf{q}_2$, where G is the Bragg reflections of the underlying average $P6_3/mmc$ lattice, $\mathbf{q}_1 = [\frac{1}{3}, \frac{1}{3}, \pm\frac{1}{2}]^*$, $\mathbf{q}_2 = [\frac{1}{3}, \frac{1}{3}, \pm\frac{2}{3}]^*$, and m and n are integers. The additional scattering reflects ordering of the carbonate groups into trigonal layers between the $(Ln_2O_2^{2+})_n$ layers, but it remains open whether $\mathbf{q}_1$ and $\mathbf{q}_2$ represent two separate structures with different stacking sequences of such layers or whether they correspond to an even more complex stacking sequence. In any case, some disorder and rotational domain twinning are present. Two structure models, one for each modulation wave vector, were constructed. Rietveld-type refinements of PND data of $La_2O_2CO_3$ II were performed, approximating the complex, and at least partly disordered, stacking sequence as a two-phase mixture of the two modulated phases. Satisfactory convergence was achieved with $R_p = 6.4\%$, $R_{wp} = 8.3\%$, and $\chi^2 = 3.32$. The isothermal expansivities, α_p, for $La_2O_2CO_3$ II and $Nd_2O_2CO_3$ II between 298 and 893 K were determined as 2.92×10^{-5} and 2.70×10^{-5} K^{-1}, respectively. © 2001 Academic Press

INTRODUCTION

Rare earth oxide carbonates $Ln_2O_2CO_3$ (Ln = rare earth element) exist in three crystalline modifications (I, IA, and II). The three polymorphs are all believed to hold an arrangement of $(Ln_2O_2^{2+})_n$ layers separated by CO_3^{2-} ions (1, 2). Improved understanding of these materials is of importance in relation to the use of functional basic oxides (perovskites) in solid oxide fuel cells, permeable membranes, catalysts, etc. in CO_2-containing atmospheres.

The type I modification has square $(Ln_2O_2^{2+})_n$ layers and gives similar X-ray diffraction patterns as $Bi_2O_2CO_3$ (1). Originally, Lagercrantz and Sillen (3) described $Bi_2O_2CO_3$ from X-ray diffraction data to be tetragonal ($I4/mmm$), however, the orientation of the CO_3^{2-} groups could not be established. More recent powder neutron diffraction investigations indicate a more complex structure (4), and orthorhombic unit cells ($a_1 = b_1 = \sqrt{2}\cdot a_T$, $c_1 = 2\cdot c_T$, space group $Pna2_1$; $a_2 = 2\cdot\sqrt{2}\cdot a_T$, $b_2 = \sqrt{2}\cdot a_T$, $c_2 = c_T$, space group $Ama2$) were considered. None of these models gave acceptable R factors or realistic O–C–O bond angles (4). Greaves and Blower (4) therefore concluded that the true carbonate group representation requires an even larger unit cell. Hence, the description for $Bi_2O_2CO_3$ (and $Ln_2O_2CO_3$ I) is incomplete with respect to the carbonate groups. The nature of IA is more ambiguous, and it is described as a monoclinic distortion of form I (1, 2).

During the past decades several studies have considered the crystal structure of the type II modification (5–9). From single-crystal X-ray diffraction data, Christensen (5) described a hexagonal structure for $Nd_2O_2CO_3$ II. Powder X-ray diffraction data revealed $La_2O_2CO_3$ II to be isostructural (6). Recently Kutlu and Meyer (7) provided similar findings for $Dy_2O_2CO_3$ II on the basis of single-crystal X-ray diffraction data. According to space group $P6_3/mmc$, the following sites are occupied: C $6h$ (x, $2x$, $\frac{1}{4}$), O1 $6h$ (x, $2x$, $\frac{1}{4}$), O2 $4e$ (0, 0, z), O3 $4f$ ($\frac{1}{3}$, $\frac{2}{3}$, z), and Ln $4f$ ($\frac{1}{3}$, $\frac{2}{3}$, z). The sixfold C and O1 sites are only $\frac{1}{3}$ occupied, which implies orientational disorder for the carbonate groups arranged between the $(Ln_2O_2^{2+})_n$ layers, built by OLn_4 tetrahedra. Structural aspects are shown in Fig. 1, and this description is hereafter termed as the average model. According to this model (Table 1), the carbonate groups in $La_2O_2CO_3$ II and $Nd_2O_2CO_3$ II are rather deformed; see C–O bond lengths, O–O separations, and O–C–O bond angles in Table 2.

An exact description of the type II structure is difficult on the basis of X-ray diffraction data alone, owing to weakly scattering oxygen and carbon atoms in combination with heavy rare earth elements. Optical absorption and

[1]To whom correspondence should be addressed. E-mail: helmer.fjellvag@kjemi.uio.no.

0022-4596/01 $35.00

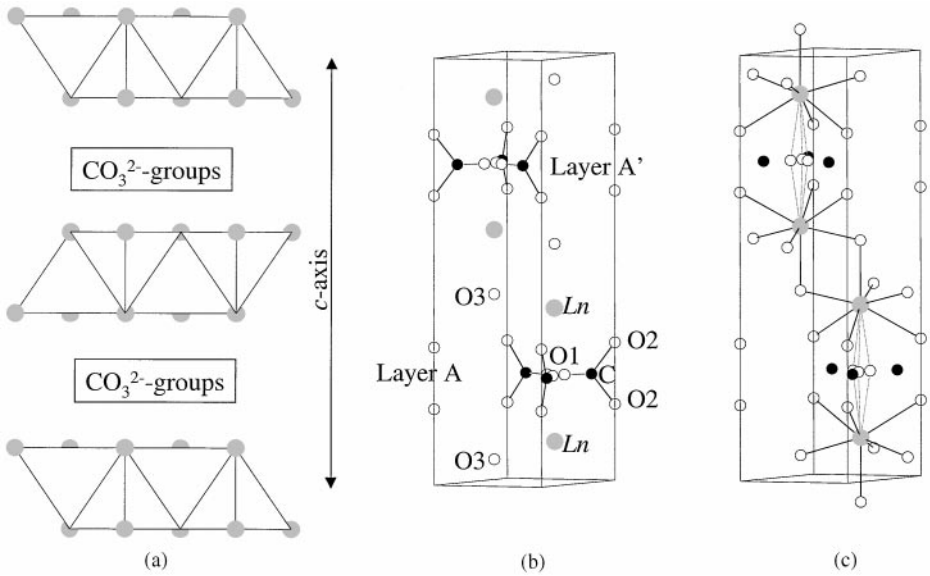

FIG. 1. (a) Schematic drawing of the crystal structure of $Ln_2O_2CO_3$ II, indicating $(Ln_2O_2^{2+})_n$ layers with OLn_4 tetrahedra separated by CO_3^{2-} groups. (b, c) Average model description of $Ln_2O_2CO_3$ II in space group $P6_3/mmc$ (5–7) with emphasis on CO_3^{2-} disordered groups (b) and Ln coordination (c). The sixfold C and O1 sites are $\frac{1}{3}$ occupied. ● Ln; ○ oxygen; ● carbon.

fluorescence spectroscopy data (8, 9) indicate that the Ln atoms (Ln = La, Nd) take more than one local coordination. The Ln sites are similar but subject to somewhat different electric fields, which may indicate different modes of packing of CO_3^{2-} ions from one layer to the next (9). For some samples, the electron diffraction patterns indicate an enlarged hexagonal unit cell, $a_{TEM} = a_{XRD} \cdot \sqrt{3}$ (8).

The planar D_{3h} symmetry of the free carbonate ion gives rise to six internal vibration modes, two of them doubly degenerate. Following the Herzberg convention, these are $\nu_1 = 1063$, $\nu_2 = 879$, $\nu_3 = 1415$, and $\nu_4 = 680\,cm^{-1}$ (10). The symmetrical stretching mode ν_1 is infrared inactive for the free ion. Its observation for many solids indicates a dipole and symmetry lowering within the carbonate group to C_{2v} or C_s (1). For $La_2O_2CO_3$ II and $Nd_2O_2CO_3$ II ν_1 is observed at 1088 and 1094 cm^{-1} (11). According to Reeder (12), the geometry of the CO_3^{2-} group is remarkably uniform in most solids despite the wide variety of crystal structures of minerals and synthetic carbonates. The O–C–O bond angle is often close to 120° and the C–O bonds vary between 125 and 131 pm (12).

Two important questions are addressed with respect to the crystal structure of $Ln_2O_2CO_3$ II. First, are the carbonate groups as strongly deformed as reported (cf. Table 2)? Second, does an ordering of the carbonate groups take place? In the present work these questions are approached for the type II crystal structures of $La_2O_2CO_3$ and $Nd_2O_2CO_3$ by means of high-resolution powder neutron

TABLE 1

Reported Unit Cell Dimensions and Fractional Atomic Coordinates for the Average Model Descriptions of $La_2O_2CO_3$ II (6), $Nd_2O_2CO_3$ II (5), and $Dy_2O_2CO_3$ II (7), Space Group $P6_3/mmc$

	Wückoff site[a]	$La_2O_2CO_3$ II	$Nd_2O_2CO_3$ II	$Dy_2O_2CO_3$ II
a (pm)		407.55(6)	399.1	386.9(2)
c (pm)		1595.7(1)	1566	1516.3(3)
x(C)[b]	6h	0.040(6)	0.13(3)	0.0843(20)
x(O1)[b]	6h	0.235(2)	0.28(3)	0.2743(7)
z(O2)	4e	0.1786(4)	0.178(3)	0.1758(3)
z(O3)	4f	0.5577(3)	0.557(2)	0.5563(6)
z(Ln)	4f	0.09570(4)	0.0944(1)	0.0938(1)

[a]Wückoff sites: 6h (x, 2x, $\frac{1}{4}$); 4e (0, 0, z); 4f ($\frac{1}{3}$, $\frac{2}{3}$, z). [b]$\frac{1}{3}$ occupied.

TABLE 2

Calculated Interatomic Separations (pm) and Bond Angles (°) for the CO_3^{2-} Groups in the Average Model Description of $La_2O_2CO_3$ II, $Nd_2O_2CO_3$ II, and $Dy_2O_2CO_3$ II

	$La_2O_2CO_3$ II	$Nd_2O_2CO_3$ II	$Dy_2O_2CO_3$ II
C–O1 (pm)	137.2	103.1	127.3
C–O2 (pm) (×2)	119.3	144.1	125.9
O1–O2 (pm) (×2)	201.9	223.3	215.5
O2–O2 (pm)	231.9	226.1	225.0
∠O1–C–O2 (°) (×2)	103.6	128.4	116.7
∠O2–C–O2 (°)	152.7	103.3	126.6

Note. Calculated on the basis of structure data in Refs. (5–7).

(PND) and synchrotron X-ray diffraction (SXRD) investigations combined with selected area electron diffraction (SAED) studies.

EXPERIMENTAL

Syntheses. $La_2O_2CO_3$ II was prepared by carbonatization of La_2O_3 (99.99%, Molycorp) under a stream of carbon dioxide at 1123 K for 5 days. $Nd_2O_2CO_3$ II was synthesized by decomposition of Nd(III)acetate hydrate (99.9%, Aldrich) at 773 K in air for 24 h. The obtained pale blue powder was thereafter cold pressed into pellets and fired for 5 more days at 1038 K under flowing carbon dioxide. All products were cooled to ambient temperature in a desiccator to prevent adsorption of water.

Powder diffraction. The sample purity was ascertained from powder X-ray diffraction data (Guinier–Hägg technique at 298 K; Cr$K\alpha_1$ and Cu$K\alpha_1$ radiation with $\lambda = 228.970$ and 154.0598 pm; silicon (13) as the internal standard). Unit cell dimensions were refined by means of the CELLKANT program (14).

High-temperature powder X-ray diffraction (HT-XRD) data were collected with a Siemens D500 diffractometer in Bragg–Brentano geometry using Cu$K\alpha_1$ radiation, a primary monochromator, and a scintillation detector. Temperature calibration was done by means of thermal expansion data for silver (15).

SXRD data for $Nd_2O_2CO_3$ II at 298 K were collected at the Swiss Norwegian Beam Lines (BM01) at ESRF (Grenoble, France). The sample was kept in a rotating glass capillary with 0.5-mm diameter. Data were measured in Debye–Scherrer mode between $2\theta = 15.00°$ and $2\theta = 80.00°$ in steps of $\Delta(2\theta) = 0.015°$ (4333 data points; 106 reflections for the average model). Monochromatic X-rays, $\lambda = 105.29$ pm, were obtained from a channel-cut Si(111) crystal.

High-resolution PND data for $La_2O_2CO_3$ II were collected at 298 K between $2\theta = 10.00°$ and $2\theta = 130.00°$ in steps of $\Delta(2\theta) = 0.05°$ (2399 data points) using the two-axis powder diffractometer PUS at the JEEP II reactor (Kjeller, Norway). Monochromatic neutrons with $\lambda = 155.28$ pm were obtained from a Ge(511) monochromator. In addition, PND data were collected for $Nd_2O_2CO_3$ II between $2\theta = 6.00°$ and $2\theta = 101.00°$ using the OPUS III two-axis

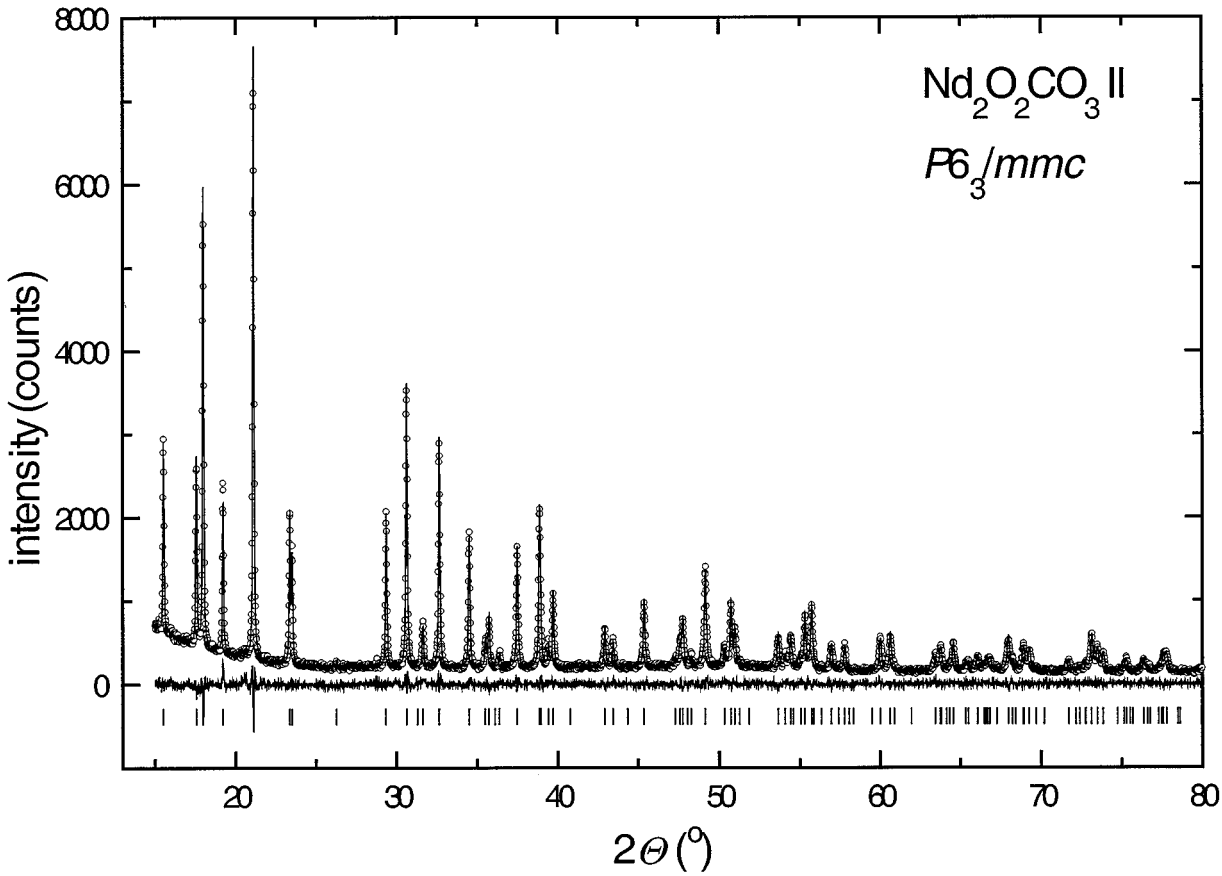

FIG. 2. Observed, calculated, and difference SXRD intensity profiles for $Nd_2O_2CO_3$ II at 298 K ($\lambda = 105.29$ pm). Refinements according to the average model with restrained carbonate groups, $F = 1000$.

diffractometer ($\lambda = 182.5$ pm; 1899 data points, 81 reflections in average model). The samples were contained in cylindrical sample holders of vanadium sealed with an indium washer.

The GSAS program (16) was used for Rietveld-type refinements of SXRD and PND data. For the PND data, the peak shape was modeled using a Gaussian function whereas for the SXRD data a pseudo-Voigt function was used,

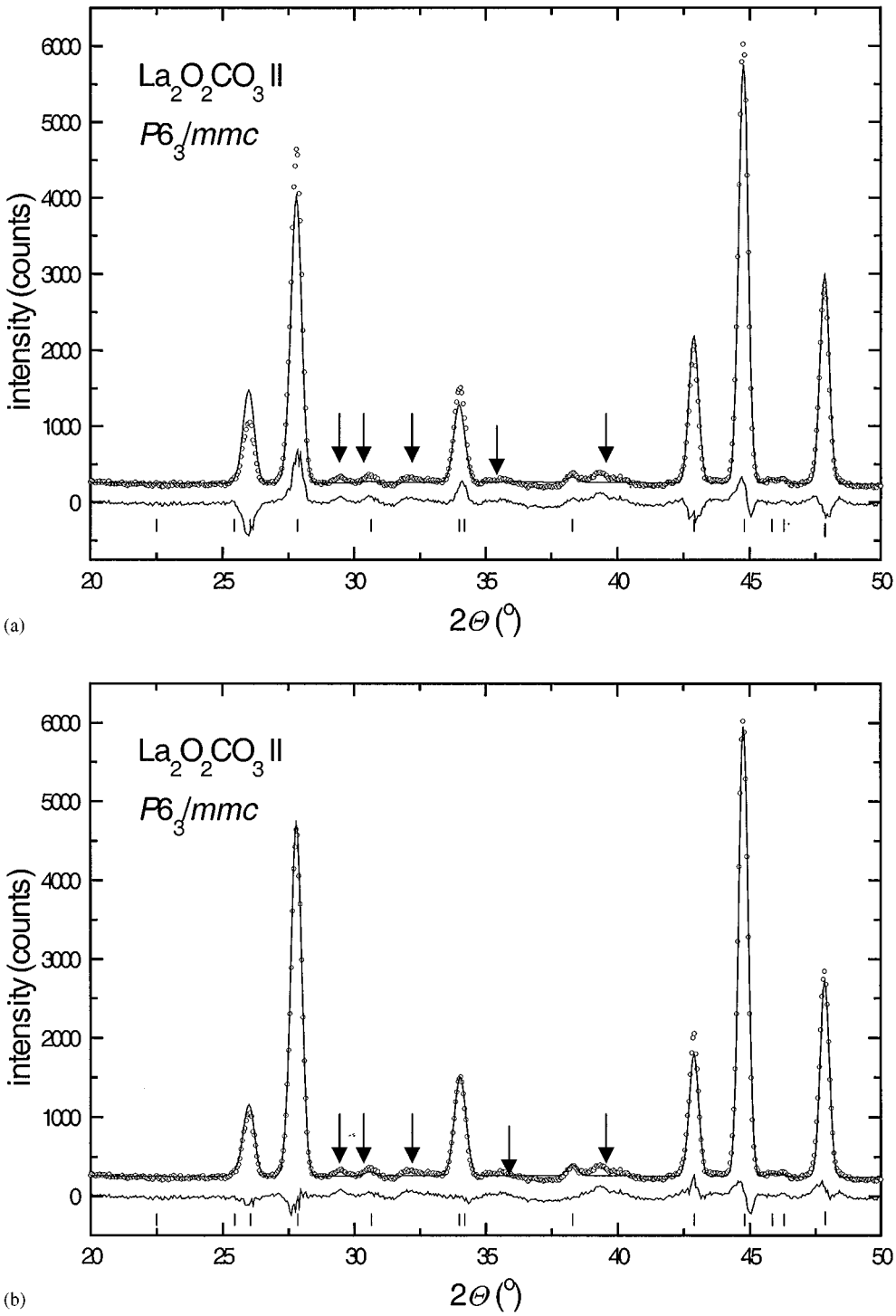

FIG. 3. Selected part of the observed, calculated, and difference PND intensity profiles for $La_2O_2CO_3$ II at 298 K ($\lambda = 155.28$ pm). Refinements according to the average model with (a) the carbonate groups restrained, $F = 1000$ and (b) relaxed restraints, $F = 1$. Arrows mark reflections not indexed on the hexagonal subcell. Similar features are observed for $Nd_2O_2CO_3$II.

including also Scherrer and strain broadening coefficients. The background was generally modeled using cosine Fourier series polynomials. The neutron scattering lengths $b_{La} = 8.27$ fm, $b_{Nd} = 7.69$ fm, $b_O = 5.81$ fm, and $b_C = 6.65$ fm were taken from the GSAS library (16). The use of soft distance restraints is described below. The PND refinements for $La_2O_2CO_3$ II included 130 reflections in the average model (1688 for model 1 in *Ama*2 and 1529 for model 2 in *C*2/*c*, see below) with 27 free refinable parameters (97 and 59 for *Ama*2 and *C*2/*c*, respectively).

Electron diffraction. SAED experiments were performed using a JEOL 2000FX transmission electron microscope. The probe specimens were prepared by mild grinding of the powdered samples before dispersing them into holey carbon-coated copper grids.

RESULTS AND DISCUSSION

Crystal structure. The synchrotron and conventional XRD patterns for $Nd_2O_2CO_3$ II and $La_2O_2CO_3$ II were completely indexed on the hexagonal unit cells described by Christensen (5) and Attfield and Ferey (6).

The SXRD data for $Nd_2O_2CO_3$ II were refined on the basis of the average model (5–7). According to Reeder (12), carbonate groups tend typically to be regular. For that reason the approach by Christensen (5) and Attfield and Ferey (6) was modified by restraining C–O bonds lengths

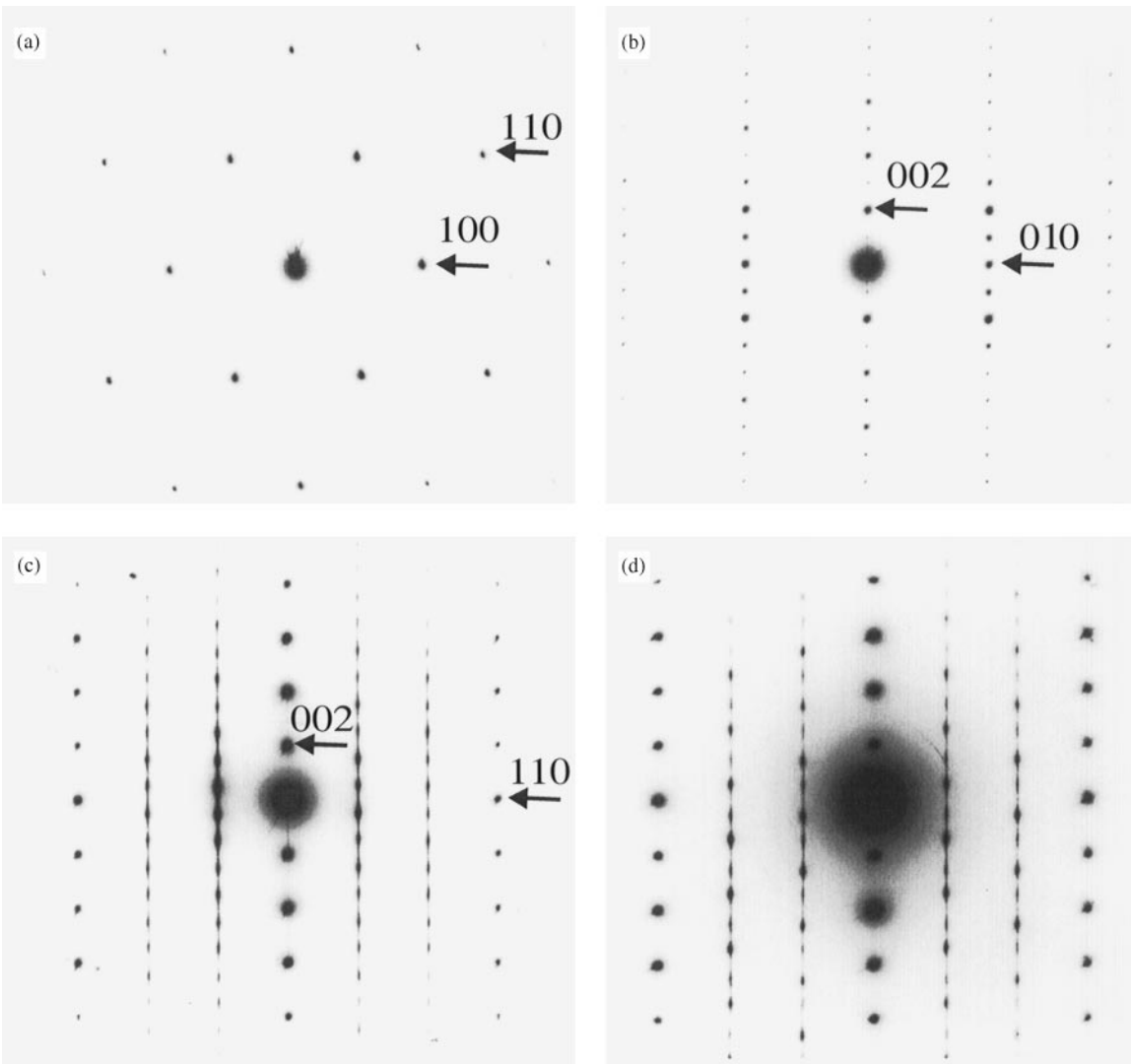

FIG. 4. SAED patterns of $La_2O_2CO_3$ II along (a) ⟨001⟩, (b) ⟨100⟩, and (c, d) ⟨1$\bar{1}$0⟩ zone axis. (c) and (d) refers to neighboring specimen areas. The appearance of not very well defined spots or spots elongation along the **c*** axis is caused by the narrow distribution of the spots. Similar features are observed for $Nd_2O_2CO_3$ II.

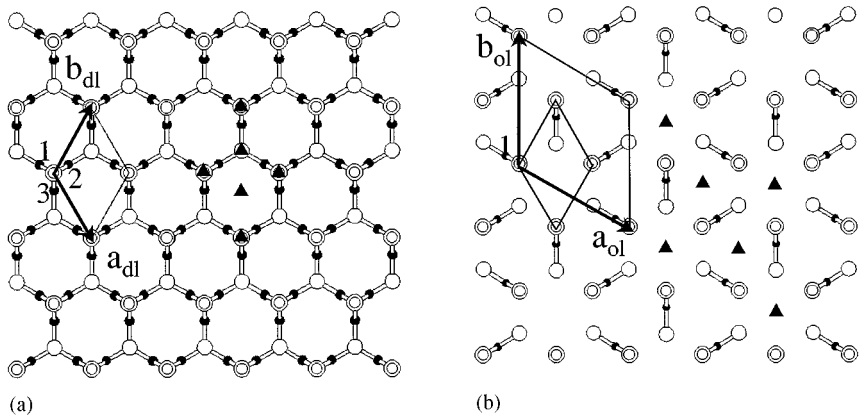

FIG. 5. (a) Disordered carbonate layer (plane group $p3m1$) according to the average model and with two-dimensional unit cell ($\mathbf{a}_{dl}$, $\mathbf{b}_{dl}$); (b) two-dimensional unit cell ($\mathbf{a}_{ol}$, $\mathbf{b}_{ol}$) of an ordered layer (plane group $p31m$); ● carbon; ○ and ○ oxygen; ▲ threefold axis.

and O–O separations (and thereby O–C–O bond angles) to 128 ± 1 and 222 ± 2 pm, respectively. Due to the observation of the symmetrical stretching mode ν_1 for the two oxide carbonates (11), the soft constraint weight was set to $F = 1000$ (16), which will allow small deviations from the ideal (restrained) bond values. The subsequent refinements converged satisfactorily, giving $R_p = 5.3\%$, $R_{wp} = 6.7\%$, and $\chi^2 = 1.54$; see observed, calculated, and difference SXRD intensity profiles in Fig. 2. No additional reflections are observed. Since earlier structure analyses (5, 6) report deformed carbonate groups (Table 2), the soft constraint weight was relaxed to $F = 1$. Again, the refinements converged well, this time giving deformed carbonate groups consistent with earlier reports (5, 6), however, without major improvement in the R factors ($R_p = 5.1\%$, $R_{wp} = 6.5\%$, and $\chi^2 = 1.44$). There is hence no support from SXRD data for deformed carbonate units. However, the data definitely proves that the basic structure with respect to the $(Nd_2O_2^{2+})_n$ layers is correct.

Thereafter the PND data for $La_2O_2CO_3$ II and $Nd_2O_2CO_3$ II were refined according to the average model with restrained carbonate groups as earlier outlined, $F = 1000$. The refinements gave for $La_2O_2CO_3$ II $R_p = 12.9\%$, $R_{wp} = 16.9\%$, and $\chi^2 = 14.4$. The apparently better fit for $Nd_2O_2CO_3$ II, $R_p = 6.6\%$, $R_{wp} = 8.5\%$, and $\chi^2 = 2.60$, is an artifact due to reduced counting statistics and resolution in the PND data (i.e., the use of an inferior diffractometer). Figure 3a shows a selected part of the PND intensity profiles for $La_2O_2CO_3$ II. Relaxation of the weight ($F = 1$) for the C–O distance and the O–O separation restraints improves significantly the fit between observed and calculated intensity profiles; e.g., for $La_2O_2CO_3$ II the

TABLE 3
Crystal Structure Data for $La_2O_2CO_3$ II and $Nd_2O_2CO_3$ II

	$La_2O_2CO_3$ II (PND, 298 K)	$La_2O_2CO_3$ II (PND, 298 K)	$La_2O_2CO_3$ II (PND, 298 K)	$Nd_2O_2CO_3$ II (SXRD, 298 K)
Crystal system	Hexagonal[a]	Orthorhombic[b]	Monoclinic[c]	Hexagonal[a]
Space group	$P6_3/mmc$	$Ama2$	$C2/c$	$P6_3/mmc$
a (pm)	407.95 (3)	3191.4 (2)	1223.9 (2)	398.805 (5)
b (pm)		1224.7 (2)	706.68 (9)	
c (pm)	1595.3 (1)	706.3 (1)	1646.5 (1)	1561.19 (2)
β (°)			75.69 (1)	
V (10^6 pm^3)	229.93 (3)	2760.7 (5)	1379.9 (2)	215.04 (1)
R_p (%)	12.9	7.3	8.4	5.3
R_{wp} (%)	16.9	9.9	10.7	6.7
χ^2	14.4	4.88	6.06	1.54

Note. Calculated standard deviations in parentheses $F = 1000$.
[a]Average model ($P6_3/mmc$).
[b]Model 1 ($Ama2$).
[c]Model 2 ($C2/c$).

TABLE 4
Fractional Atomic Coordinates for $La_2O_2CO_3$ II, Model 1, Space Group *Ama*2

Atom	Wückoff site[a]	Coordinates		
		x	*y*	*z*
C1	4*a*	0	0	0.950 (4)
C2	4*b*	$\frac{1}{4}$	0.334 (3)	0.049 (3)
C3	4*b*	$\frac{1}{4}$	0.032 (3)	0.990 (5)
C4	4*b*	$\frac{1}{4}$	0.138 (2)	0.469 (5)
C5	8*c*	−0.0003 (4)	0.685 (2)	0.039 (4)
O1	4*a*	0	0	0.768 (4)
O2	4*b*	$\frac{1}{4}$	0.340 (4)	0.230 (3)
O3	4*b*	$\frac{1}{4}$	0.627 (3)	0.415 (7)
O4	4*b*	$\frac{1}{4}$	0.044 (4)	0.387 (9)
O5	8*c*	−0.0082 (7)	0.769 (2)	0.141 (5)
O6	8*c*	0.2848 (1)	−0.018 (3)	0.012 (4)
O7	8*c*	0.0349 (1)	0.001 (2)	0.039 (4)
O8	8*c*	0.2151 (1)	0.335 (3)	−0.041 (3)
O9	8*c*	0.7151 (1)	0.322 (2)	0.027 (5)
O10	8*c*	0.4619 (4)	0.661 (2)	0.011 (4)
O11	8*c*	0.9696 (5)	0.623 (2)	−0.012 (4)
O12	8*c*	0.0974 (7)	−0.002 (3)	0.336 (6)
O13	8*c*	0.344 (1)	−0.010 (3)	0.681 (7)
O14	8*c*	0.400 (1)	0.331 (4)	0.333 (5)
O15	8*c*	0.899 (1)	0.331 (3)	0.328 (6)
O16	8*c*	0.1579 (8)	0.667 (3)	0.682 (5)
O17	8*c*	0.6548 (9)	0.671 (3)	0.655 (6)
La1	8*c*	0.3277 (6)	−0.009 (2)	0.342 (6)
La2	8*c*	0.0766 (9)	0.008 (2)	0.667 (5)
La3	8*c*	0.1719 (9)	0.327 (3)	0.346 (4)
La4	8*c*	0.6710 (9)	0.339 (3)	0.345 (5)
La5	8*c*	0.4233 (6)	0.665 (2)	0.659 (4)
La6	8*c*	0.9238 (6)	0.665 (2)	0.681 (4)

Note. Calculated standard deviations in parentheses. Isotropic displacement factors (in 10^4 pm^2): $B_{iso}(C) = 1.426$, $B_{iso}(O) = 1.444$, and $B_{iso}(La) = 0.091$. $F = 1000$.

[a]Wückoff sites: 4*a* (0, 0, *z*); 4*b* ($\frac{1}{4}$, *y*, *z*); 8*c* (*x*, *y*, *z*).

TABLE 5
Fractional Atomic Coordinates for $La_2O_2CO_3$ II, Model 2, Space Group *C*2/*c*

Atom	Wückoff site[a]	Coordinates		
		x	*y*	*z*
C1	4*e*	0	0.820 (2)	$\frac{1}{4}$
C2	8*f*	0.693 (1)	0.283 (2)	−0.2535 (5)
O1	4*e*	0	0.002 (2)	$\frac{1}{4}$
O2	8*f*	0.7773 (9)	0.601 (2)	0.2423 (9)
O3	8*f*	0.8416 (9)	0.310 (2)	0.1857 (5)
O4	8*f*	0.517 (1)	0.233 (2)	0.1799 (2)
O5	8*f*	0.175 (1)	0.271 (2)	0.1770 (5)
O6	8*f*	0.900 (2)	0.084 (4)	0.5574 (8)
O7	8*f*	0.563 (2)	0.083 (3)	0.5558 (8)
O8	8*f*	0.234 (2)	0.076 (3)	0.5579 (8)
La1	8*f*	0.055 (1)	0.092 (3)	0.0946 (6)
La2	8*f*	0.717 (1)	0.087 (2)	0.0940 (5)
La3	8*f*	0.385 (1)	0.091 (2)	0.0963 (6)

Note. Calculated standard deviations in parentheses. Isotropic displacement factors (in 10^4 pm^2): $B_{iso}(C) = 1.308$, $B_{iso}(O) = 0.355$, and $B_{iso}(La) = 0.529$. $F = 1000$.

[a]Wückoff sites: 4*e* (0, *y*, $\frac{1}{4}$); 8*f* (*x*, *y*, *z*).

reliability factors became $R_p = 8.7\%$, $R_{wp} = 11.3\%$, and $\chi^2 = 6.20$ (for fit, see Fig. 3b). However, the improved fit of the main reflections does not necessarily indicate strongly deformed carbonate groups. In the present case the adopted model is incomplete and a more complex model with ordering of carbonate groups is required. In this sense the findings concur with those for the closely related compound $Bi_2O_2CO_3$ (4).

The PND patterns for both $La_2O_2CO_3$ II and $Nd_2O_2CO_3$ II contain weak additional reflections that cannot be described by the small hexagonal unit cell (see reflections marked by arrows in Figs. 3a and 3b for $La_2O_2CO_3$ II) nor do they correspond to any known impurity. Since $La_2O_2CO_3$ II is diamagnetic and $Nd_2O_2CO_3$ II paramagnetic at 298 K (11), magnetic scattering contributions can be ruled out. Carbon and oxygen have quite large neutron scattering lengths, therefore it is likely that the additional peaks reflect carbonate ordering. To explain these additional, weak reflections in the PND patterns, SAED was applied.

When crystallites of $Ln_2O_2CO_3$ II (*Ln* = La or Nd) were aligned along the zone axis ⟨001⟩ (Fig. 4a) or ⟨100⟩ (Fig. 4b), the SAED patterns in the TEM studies revealed

TABLE 6
Selected Interatomic Distances (pm) and Bond Angles (°) for Carbonate Groups in $La_2O_2CO_3$ II, Model 1 (*Ama*2) and Model 2 (*C*2/*c*) as Derived from PND Data

Distances (pm)		Angles (°)	
		Carbonate groups, Model 1	
C1–O1	128.5 (4)	∠O1–C1–O7	119.4 (3) × 2
C1–O7	127.8 (2) × 2	∠O7–C1–O7	121.2 (6)
C2–O2	128.4 (4)	∠O2–C2–O8	119.3 (4) × 2
C2–O8	128.0 (3) × 2	∠O8–C2–O8	121.0 (7)
C3–O3	128.5 (4)	∠O3–C3–O6	119.2 (5) × 2
C3–O6	128.0 (3) × 2	∠O6–C3–O6	120.6 (7)
C4–O4	128.5 (4)	∠O4–C4–O9	118.8 (5) × 2
C4–O9	128.1 (3) × 2	∠O9–C4–O9	120.6 (8)
C5–O5	128.9 (4)	∠O5–C5–O10	117.6 (6)
C5–O10	127.6 (4)	∠O5–C5–O11	119.3 (6)
C5–O11	127.5 (4)	∠O10–C5–O11	122.7 (7)
		Carbonate groups, Model 2	
C1–O1	128.8 (4)	∠O1–C1–O4	118.6 (3) × 2
C1–O4	127.7 (3) × 2	∠O4–C1–O4	122.8 (7)
C2–O2	130.3 (4)	∠O2–C2–O3	117.2 (6)
C2–O3	127.5 (4)	∠O2–C2–O5	116.7 (7)
C2–O5	127.7 (4)	∠O3–C2–O5	122.5 (7)

Note. $F = 1000$.

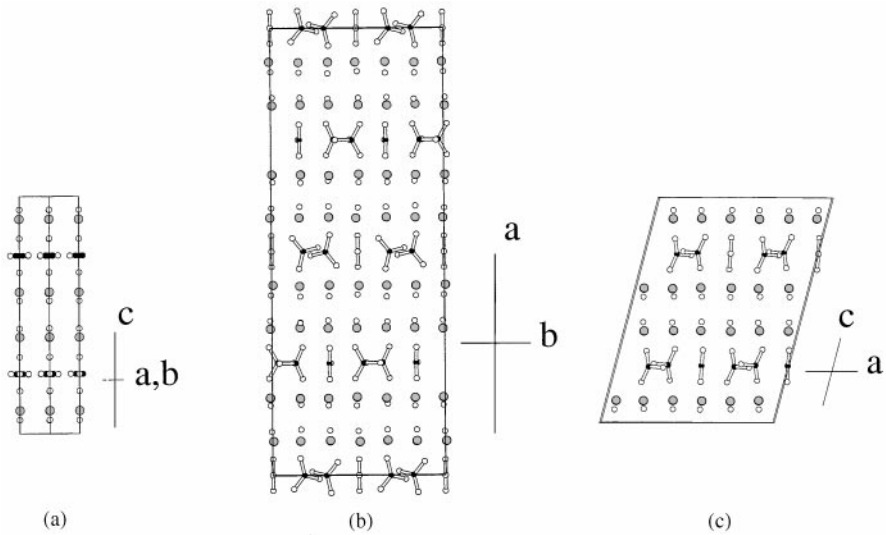

FIG. 6. The crystal structure of $Ln_2O_2CO_3$ II (Ln = La, Nd) according to (a) the average model ($P6_3/mmc$) seen along [110], (b) model 1 ($Ama2$) seen along [001], and (c) model 2 ($C2/c$) seen along [010].

a reciprocal lattice compatible with the average structure described in space group $P6_3/mmc$, Table 1. In contrast, SAED patterns along other directions showed considerable amounts of additional scattering. Figures 4c and 4d show typical SAED patterns along the $\langle 1\bar{1}0\rangle$ zone axis collected for the same specimen. Note that the additional scattering is different in the two diffraction patterns, which demonstrates a variation of the reciprocal lattice upon moving the electron beam over the crystallite or from crystallite to crystallite. However, all observed scattering in addition to **G** (the Bragg lattice of the average model with disordered carbonate groups) could always be explained as falling on the lines $\mathbf{G} \pm \langle \frac{1}{3}, \frac{1}{3}, l\rangle^*$. The additional scattering is in the form of very narrowly distributed but essentially discrete spots.

After a large number of SAED patterns from different crystallites was studied, it was concluded that the dominant part of the scattering can be described as $\mathbf{H} = \mathbf{G} \pm m\mathbf{q}_1 + n\mathbf{q}_2$, where $\mathbf{q}_1 = [\frac{1}{3}, \frac{1}{3}, \pm\frac{1}{2}]^*$ and $\mathbf{q}_2 = [\frac{1}{3}, \frac{1}{3}, \pm\frac{2}{3}]^*$ are modulation wave vectors and m and n are integers. The variations in the appearance of the SAED patterns in Figs. 4c and 4d can be explained by different relative intensities (amounts) of these modulation wave vectors. All examined crystallites contained both types of modulation wave vectors, however, in varying proportions.

These features in reciprocal space gave important indications on the real space ordered crystal structure. First, the fact that the reciprocal space includes only features described with $\mathbf{G} \pm \langle \frac{1}{3}, \frac{1}{3}, l\rangle^*$ indicates that each partially occupied disordered carbonate layer (in the average model) could be decomposed into fully occupied trigonal layers with an expanded two-dimensional lattice repetition. If one assumes that the structure consists of ordered CO_3^{2-} triangles, only one of the three carbon atoms surrounding each indicated oxygen (cf. Fig. 5a) could locally be present. If the threefold axes at (0, 0) and $(\frac{1}{3}, \frac{2}{3})$ in the $p3m1$ plane group of the projected disordered layer (dl) is removed, the two-dimensional unit cell is expanded and the plane group is changed to $p31m$ (cf. Fig. 5b). The two-dimensional unit cell of this ordered layer (ol) can be expressed as $\mathbf{a}_{ol} = \mathbf{2a}_{dl} + \mathbf{b}_{dl}$ and $\mathbf{b}_{ol} = -\mathbf{a}_{dl} + \mathbf{b}_{dl}$ (corresponding to $\mathbf{a}^*_{ol} = \frac{1}{3}\mathbf{a}^*_{dl} + \frac{1}{3}\mathbf{b}^*_{dl}$ and $\mathbf{b}^*_{ol} = -\frac{1}{3}\mathbf{a}^*_{dl} + \frac{2}{3}\mathbf{b}^*_{dl}$).

In the crystal structure, only one of these ordered layers is present at a given height along **c**. The removal of the threefold axis (actually the 6_3 operation) implies three possible stacking rotations of each ordered layer. These are indicated in Fig. 5a as 1, 2, or 3. Rotation 1 is drawn in Fig. 5b.

In the unit cell of the average model, there are two symmetry-related disordered CO_3^{2-} layers (A and A') separated by $(Ln_2O_2^{2+})_n$ slabs (Figs. 1 and 5). When each layer is allowed to consist of one set of each of the three different configurations (A = 1, 2, 3 and A' = 1′, 2′, 3′), an unlimited number of stacking sequences may be created. If the stacking sequence of these layers is totally ordered, l will lock into a fixed value and a superstructure is formed. If there is a certain disorder related to this sequence, narrowly distributed spots or streaking will appear along **c***.

In an attempt to define a structure model that can be refined with respect to the available high-resolution powder neutron diffraction data for $La_2O_2CO_3$ II, it was assumed that each of the two observed modulation wave vectors, i.e., $\mathbf{q}_1 = [\frac{1}{3}, \frac{1}{3}, \pm\frac{1}{2}]^*$ and $\mathbf{q}_2 = [\frac{1}{3}, \frac{1}{3}, \pm\frac{2}{3}]^*$, correspond to a frequently appearing stacking sequence. A unit cell and space group were assigned to each to evaluate the

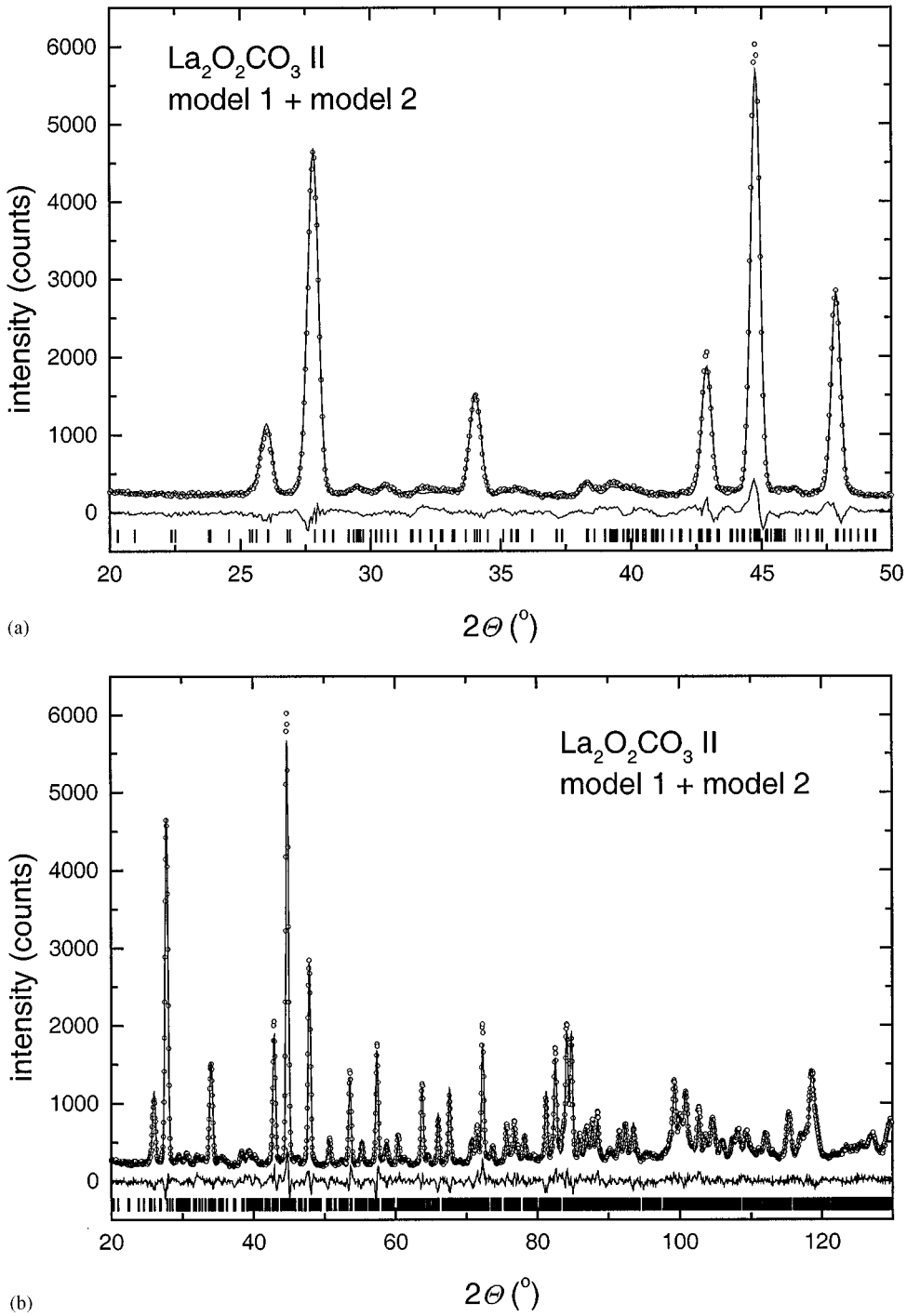

FIG. 7. Observed, calculated, and difference PND intensity profiles for $La_2O_2CO_3$ II at 298 K ($\lambda = 155.28$ pm); models 1 and 2, refined as a two-phase with restrained carbonate groups, $F = 1000$; (a) selected region; (b) whole pattern.

hypothesis of stacked hexagonal nets. Note that the choice of these two models does not imply that there are no other repeated stacking sequences. In relation to the diffraction patterns, one should bear in mind that domain twinning, intergrowths of the two proposed sequences, and stacking disorder appear to be present on a fine scale. Therefore, the derived crystal structures should not be considered as exact at this stage.

Model 1 was constructed to explain the modulation wave vector $\mathbf{q}_1 = [\frac{1}{3}, \frac{1}{3}, \pm\frac{1}{2}]^*$. The stacking sequence 12′13′1

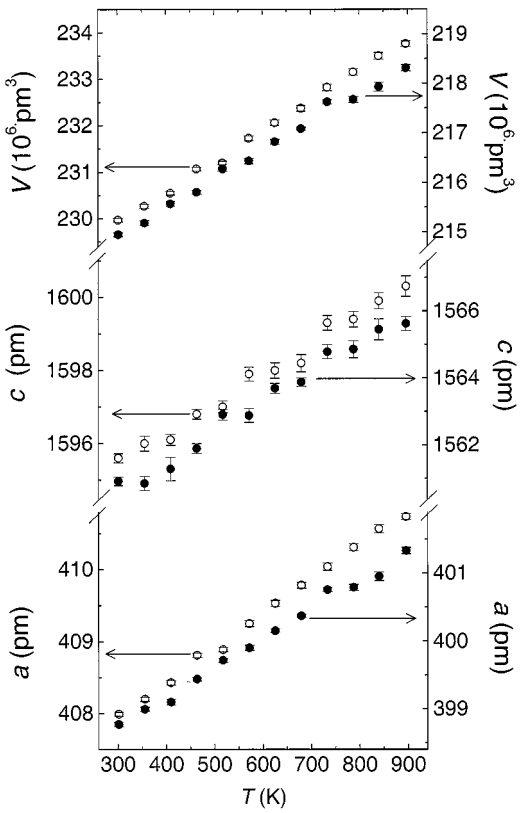

FIG. 8. Temperature dependence of a, c, and V for average unit cell of $La_2O_2CO_3$ II (open symbols, ○) and $Nd_2O_2CO_3$ II (solid symbols, ●).

(Fig. 5) was chosen. Model 1 is described in the orthorhombic space group *Ama*2, with the unit cell $\mathbf{a}_1 = 2\mathbf{c}$, $\mathbf{b}_1 = 3\mathbf{b}$, and $\mathbf{c}_1 = -\mathbf{2a} - \mathbf{b}$ (**a**, **b**, and **c** refer to the average model) and there are 28 nonequivalent atoms in the asymmetric unit. Model 2 was constructed to explain the modulation wave vector $\mathbf{q}_2 = [\frac{1}{3}, \frac{1}{3}, \pm\frac{2}{3}]^*$. The stacking sequence of the layers is 11′22′33′1 (Fig. 5). Model 2 is described in the monoclinic space group $C2/c$ with the unit cell $\mathbf{a}_2 = -3\mathbf{a} - 3\mathbf{b}$, $\mathbf{b}_2 = \mathbf{a} - \mathbf{b}$, and $\mathbf{c}_2 = -\mathbf{a} - \mathbf{b} + \mathbf{c}$ and there are 13 nonequivalent atoms in the asymmetric unit.

Models 1 and 2 were first refined separately using high-resolution PND data for $La_2O_2CO_3$ II. The carbonate groups in the two models were constrained as earlier outlined, $F = 1000$. The refinements converged well, giving for model 1 $R_p = 7.3\%$, $R_{wp} = 9.9\%$, and $\chi^2 = 4.88$ and for model 2 $R_p = 8.4\%$, $R_{wp} = 10.7\%$, and $\chi^2 = 6.06$. Results and derived structure data are given in Tables 3–6. Figure 6 shows, in addition to the average model, the two superstructures resulting from the modulations for models 1 and 2. Both refined models maintain rather regular carbonate groups (Table 6). For model 1 the La–O bonds in the $(La_2O_2^{2+})_n$ layers with OLa_4 tetrahedra are in the range 222(4)–260(3) pm, whereas the corresponding values are 238(3)–248(2) pm for model 2. The refined unit cell dimensions for models 1 and 2 concur well with those of the average model after appropriate conversion (see Table 3).

According to the SAED experiments, all crystallites gave rise to satellites described with both $\mathbf{q}_1$ and $\mathbf{q}_2$. This could indicate an even more complex stacking sequence with domains twinned by rotation around the hexagonal axis, giving the different appearance of SAED from different areas of the crystallites. Further details may possibly be deduced by means of high-resolution electron microscopy (HREM). The picture with two phases were tested out during Rietveld-type refinements of the PND data for $La_2O_2CO_3$ II as a first approach, i.e., phase modulation 1 described by the unit cell according to $\mathbf{q}_1$ and modulation 2 as described by the unit cell according to $\mathbf{q}_2$. The structural parameters determined in the individual refinements of models 1 and 2 were used as input parameters, however, being kept constant during the entire process where only the mass fraction between the two models was refined, giving a value of 0.68. The two-phase refinements gave a considerably improved fit ($R_p = 6.4\%$, $R_{wp} = 8.3\%$, and $\chi^2 = 3.32$). A selected part of the observed, calculated, and difference intensity profiles for the PND data of $La_2O_2CO_3$ II is given in Fig. 7a; the whole pattern is shown in Fig. 7b.

Thermal expansion. The thermal expansions of $La_2O_2CO_3$ II and $Nd_2O_2CO_3$ II were determined by HT-XRD between 298 and 893 K on the basis of the average model ($P6_3/mmc$). No internal standard was used in the measurements and the calculated unit cell dimensions at 298 K were slightly adjusted to comply with values derived from Guinier–Hägg data. The temperature dependencies of a, c, and V are shown in Fig. 8. The isobaric volume expansivities, α_p, for $La_2O_2CO_3$ II and $Nd_2O_2CO_3$ II were established from the approximately linear $V(T)$ curves. For the temperature range 298–893 K, $\alpha_p = (1/V_T)\cdot(\Delta V/\Delta T)$ are 2.92×10^{-5} and 2.70×10^{-5} K^{-1}, respectively.

ACKNOWLEDGMENTS

Contribution from the Swiss Norwegian Beam Lines at ESRF (Grenoble, France). Financial support from the Swedish Natural Science Research Council (NFR) is gratefully acknowledged (AKL).

REFERENCES

1. R. P. Turcotte, J. O. Sawyer, and L. Eyring, *Inorg. Chem.* **8,** 238 (1969).
2. J. O. Sawyer, P. Caro, and L. Eyring, *Monatsh. Chem.* **102,** 333 (1971).
3. A. Lagercrantz and L. G. Sillen, *Ark. Kem. Miner. Geol. A* **25,** 1 (1948).
4. C. Greaves and S. K. Blower, *Mater. Res. Bull.* **23,** 1001 (1988).
5. A. N. Christensen, *Acta Chem. Scand.* **24,** 2440 (1970).
6. J. P. Attfield and G. Ferey, *J. Solid State Chem.* **82,** 132 (1989).
7. I. Kutlu and G. Meyer, *Z. Anorg. Allg. Chem.* **625,** 402 (1999).
8. H. Dexpert, E. Antic-Fidancev, D. R. Svoronos, and P. Caro, *J. Cryst. Spectrosc. Res.* **12,** 143 (1982).

9. O. K. Moune-Minn and P. Caro, *J. Cryst. Spectrosc. Res.* **12,** 157 (1982).
10. G. Herzberg, "Molecular Spectra and Molecular Structure, II. Infrared and Raman Spectra of Polyatomic Molecules." Van Nostrand, New York, 1945.
11. A. Olafsen, H. Fjellvåg, S. Stølen, T. Atake, H. Kawaji, and K. Matsuo, *J. Chem. Thermodyn.* **31,** 433 (1999).
12. R. J. Reeder, "Carbonates: Mineralogy and Chemistry" (R. J. Reeder, Ed.), pp. 4–7. Mineralogical Society of America, Book Crafters, Inc., Chelsea, MI, 1990.
13. M. C. Morris, H. F. McMurdie, E. H. Evans, B. Paretzkin, J. H. de Groot, C. R. Hubbard, and S. J. Carmel, *Natl. Bur. Stand.* (*U.S*) *Monogr.* 25, **13,** 35 (1976).
14. N. O. Ersson, "Program CELLKANT." Chemical Institute, University of Uppsala, Sweden, 1981.
15. J. Spreadborough and J. W. Christian, *J. Sci. Instrum.* **36,** 116 (1959).
16. A. C. Larson and R. B. Von Dreele, "Program GSAS, General Structure Analysis System." LANSCE, MS-H 805, Los Alamos National Laboratory, Los Alamos, NM, 1994.